RARE METALS

Composite polymer electrolytes reinforced by a three-dimensional polyacrylonitrile/Li$_{0.33}$La$_{0.557}$TiO$_3$ nanofiber framework for room-temperature dendrite-free all-solid-state lithium metal battery

Tian-Qi Yang, Cheng Wang, Wen-Kui Zhang* , Yang Xia, Yong-Ping Gan,
Hui Huang, Xin-Ping He, Jun Zhang*

Abstract Substituting liquid electrolytes with solid electrolytes is considered as an important strategy to solve the problem of flammability and explosion for traditional lithium-ion batteries (LIB). However, neither inorganic solid electrolytes (ISE) nor solid polymer electrolytes (SPE) alone can meet the operating requirements for room-temperature (RT) all-solid-state lithium metal batteries (ASSLMB). Here, we report a three-dimensional (3D) nanofiber framework reinforced polyethylene oxide (PEO)-based composite polymer electrolytes (CPE) through constructing a nanofiber framework combining polyacrylonitrile (PAN) and fast Li-ion conductor Li$_{0.33}$La$_{0.557}$TiO$_3$ (LLTO) framework by electrospinning method. Meanwhile, the PEO electrolyte filled in the pores of the PAN/LLTO nanofiber framework can effectively isolate the direct contact between the chemically active Ti^{4+} in LLTO with lithium metal, thereby avoiding the occurrence of interfacial reactions. Enhanced electrochemical stability makes a wide electrochemical window up to 4.8 V with an ionic conductivity of about 9.87×10^{-5} S·cm^{-1} at RT. Benefiting from the excellent lithium dendrite growth inhibition ability of 3D PAN/LLTO nanofiber framework, especially when the mass of LLTO reaches twice that of the PAN, Li/Li symmetric cell could cycle stably for 1000 h without a short circuit. In addition, under 30 °C, the LiFePO$_4$/Li ASSLMB using such CPE delivers large capacities of 156.2 and 140 mAh·g^{-1} at 0.2C and 0.5C, respectively. These results provide a new insight for the development of the next generation of safe, high-performance ASSLMBs.

Keywords Li$_{0.33}$La$_{0.557}$TiO$_3$; 3D nanofiber framework; Composite polymer electrolyte; All-solid-state lithium metal battery

T.-Q. Yang, C. Wang, W.-K. Zhang*, Y. Xia, Y.-P. Gan,
H. Huang, X.-P. He, J. Zhang*
College of Materials Science and Engineering, Zhejiang University of Technology, Hangzhou 310014, China
e-mail: msechem@zjut.edu.cn

J. Zhang
e-mail: zhangjun@zjut.edu.cn

1 Introduction

Owing to the increasing shortage of fossil fuels together with the serious environmental pollution caused by combustion, the development of new clean energy sources such as hydropower, wind energy, solar energy, and related energy storage equipment are urgently needed. Lithium-ion batteries (LIBs) have been extensively studied due to their excellent rechargeable characteristics as well as high energy density [1–3]. However, the traditional LIBs contain a large amount of organic electrolyte [4–6], which is flammable and easy to leak, always leading to serious safety accidents. Solid electrolytes can fundamentally solve the safety problem; meanwhile, higher energy density is achieved by matching with high-voltage cathode and lithium metal anode, which has an ultrahigh theoretical specific capacity (3860 mAh·g^{-1}) [7–10].

The solid electrolytes currently widely studied can be divided into two major categories, inorganic solid electrolyte (ISE) and solid polymer electrolyte (SPE) [10–13]. The room-temperature ion conductivity of sulfide type [14–18] and garnet type [19–23] electrolytes in ISE can

reach more than 1×10^{-3} S·cm^{-1}, which is close to liquid electrolytes; nonetheless, the poor compatibility of the electrolyte/electrode interface leads to lower ion and electron conduction efficiency. SPE is composed of lithium salt with low lattice energy and polymer with high dielectric constant [24], and the main advantages of SPE are flexibility, easy processing, and good interface contact with the electrode [24–26]. Yet, the ionic conductivity of SPE at room temperature is low, the lithium-ion transfer number (t_{Li}^+) is small, and the electrochemical window is narrow [27]. In addition, the especially low Young's modulus of SPE [28] makes the SPE easy to be pierced by lithium dendrites when the battery is working, causing serious safety problems. CPE perfectly combines the advantages of the ISE and SPE, and high ionic conductivity and mechanical strength of ISE are retained while having good flexibility and excellent processing properties of SPE. It is considered to be one of the favored candidates for the next generation of all-solid-state lithium metal batteries (ASSLMBs).

In recent years, CPEs based on polyethylene oxide (PEO) and polyacrylonitrile (PAN) for polymermatrices have been extensively investigated [29–33]. The polymer matrix of CPEs mainly includes PAN, PEO, polyvinylidene fluoride (PVDF), polymethyl methacrylate (PMMA), etc. [34]. Among them, PEO has low glass transition temperature and good compatibility with many lithium salts [35–37] while PAN exhibits pretty good thermal stability and mechanical properties [38–40]. In addition, the grain conductivity of LLTO can reach 1.43×10^{-3} S·cm^{-1} at room temperature [41], thus being widely used as fillers in CPE. Zhu et al. [35] prepared LLTO nanofibers for PEO/LLTO CPE by electrospinning method, and LLTO nanofibers provide continuous lithium-ion transport channels while substantially reducing the crystallinity of PEO, especially when the content of LLTO nanofibers reaches 15 wt% of PEO, CPE has a conductivity of 2.4×10^{-4} S·cm^{-1} with an electrochemical window up to 5 V (vs. Li$^+$/Li). Besides, the prepared CPE also exhibits excellent lithium dendrite suppression ability, Li/Li symmetric cell with corresponding CPE could cycle stably for 720 h without a short circuit at 25 °C with a current density of 0.5 mA·cm^{-2}. Huo et al. [36] designed a ceramic-in-polymer (CIP) electrolyte with 20 vol% 200-nm Li$_{6.4}$La$_3$Zr1.4Ta$_{0.6}$O$_{12}$ (LLZTO) particles for high ionic conductivity and a polymer-in-ceramic (PIC) electrolyte with 80 vol% 5-μm LLZTO for high tensile strength. The sandwiched CIP-PIC-CIP composite electrolytes based on the above two electrolytes maintain the advantages of both. High mechanical strength of PIC can effectively inhibit the growth of lithium dendrites. Benefiting from this, Li/Li symmetric cell could cycle stably for 400 h at 30 °C with a current density of 0.2 mA·cm^{-2}; meanwhile, ASSLMB with LiFePO$_4$ cathode shows great cycle stability with a specific capacity of 99.1 mAh·g^{-1} after 200 cycles at room temperature under 0.1C. Wan et al. [37] prepared a three-dimensional (3D) fiber-network-reinforced bicontinuous solid composite electrolyte with PAN and lithium aluminum titanium phosphate (LATP). PAN and PEO isolate the direct contact between active Ti^{4+} in LATP with lithium metal, thus avoiding the interfacial reaction. LATP/PAN fiber network constructed a 3D continuous lithium-ion transmission channel; at the same time, high mechanical strength of LATP/PAN network is also beneficial to inhibit the growth of lithium dendrites. Enhanced electrochemical stability made Li/Li symmetric cell cycle stable for 400 h at 60 °C with a current density of 0.2 mA·cm^{-2} while ASSLMB with LiFePO$_4$ cathode exhibited an ultrahigh specific capacity of 144 mAh·g^{-1} after 100 cycles at 60 °C under 0.1C. Compositing polymers with inorganic nanofillers and designing the structure of CPEs have become a mainstream research direction. However, as reported above, inorganic nanofillers reduce the crystallinity of polymers only to a limited extent. Meanwhile, these CPEs exhibit low lithium-ion transfer number at room temperature. Most CPEs still need a high temperature to enable satisfied electrochemical performance. Therefore, it is a challenging and urgent problem to develop ASSLMBS that operated at room temperature by significantly reducing the crystallinity of the polymer body and building fast lithium-ion transport channels in CPE.

Targeted at the above problems, here, we report a 3D PAN/LLTO nanofiber framework combining PAN and LLTO by electrospinning method. Furthermore, PAN/LLTO-based CPE was fabricated through compounding with a PEO, LiTFSI, SN mixed slurry, and the addition of SN can significantly reduce the crystallinity of PEO, thus increasing the conductivity of CPE by 3 orders of magnitude compared to that of pure PEO, enabling ASSLMBs to work at room temperature. PPLE2 electrolyte exhibits an ionic conductivity of about 9.87×10^{-5} S·cm^{-1} at RT with an electrochemical window of 4.8 V. Importantly, PPLE2 electrolyte can effectively inhibit the growth of lithium dendrites, thus Li/Li symmetric batteries could cycle stably for 1000 h under a current density of 0.1 mA·cm^{-2}. At the same time, ASSLMB with the LFP cathode exhibited great rate capability and demonstrated a large initial capacity of 156.2 and 140 mAh·g^{-1} under 30 °C at 0.2C and 0.5C, respectively.

2 Experimental

2.1 Preparation of Li$_{0.33}$La$_{0.557}$TiO$_3$ (LLTO) nanoparticles

LLTO nanoparticles were synthesized by the previously reported work [42]. In brief, LiNO$_3$ (99.9%, Aladdin),

La(NO$_3$)$_3$.6H$_2$O (99.99%, Aladdin), Ti(OC$_4$H$_9$)$_4$ ($\geq$ 99.0%, Aladdin) were dissolved in ethanol, according to the stoichiometric amount of 0.33: 0.557: 1, anhydrous citric acid was used as the complexing agent, then LLTO nanoparticles were synthesized by the solvothermal method; importantly, an excess of 20 wt% LiNO$_3$ was added to compensate for the Li-loss during the calcination process. After being rinsed several times with alcohol, the dried sample was maintained at 350 °C for 4 h and then calcined 900 °C for 2 h with a heating rate of 5 °C·min^{-1}, respectively. Finally, after cooling to room temperature, LLTO nanoparticles were obtained through ground in an agate mortar.

2.2 Preparation of 3D PAN/LLTO nanofiber framework

The 3D PAN/LLTO nanofiber framework was gained by the electrospinning method. Firstly, 10 wt% PAN was dissolved into N,N-dimethylformamide (DMF, AR, 99.5%, Aladdin) to form a pale-yellow transparent solution, which represents pure PAN. Afterwards, LLTO nanoparticles were added with different mass ratios of PAN to LLTO (1:1, 1:2, and 1:3) and stirred overnight to obtain a uniform precursor. The electrospinning process was carried out with a feed rate of 0.6 ml·h^{-1}, a voltage of 15 kV, and a distance of 15 cm from the needle to the roller collector. Then the framework was dried at 80 °C in a vacuum oven for overnight to remove the residual solvent. 3D PAN/LLTO nanofiber frameworks were named as PNF, PLNF1, PLNF2, and PLNF3 according to the mass ratio of PAN to LLTO, respectively.

2.3 Preparation of PAN/LLTO-based CPE

The PAN/LLTO-based CPE was prepared by the solution casting method. PEO (molecular weight, MW = 600,000, Aladdin), bistri-fluoromethanesulfonamide lithium salt (LiTFSI, Aladdin, 99%), and succinonitrile (SN, Aladdin, 99%) were dissolved in acetonitrile (ACN, AR, > 99%, Aladdin) and mix thoroughly to form a homogeneous slurry, in which the molar ratio of ethylene oxide (EO) to LiTFSI was 12: 1 and the mass ratio of PEO to SN was 15: 1. Then the slurry was dropped on the surface of the 3D PAN/LLTO nanofiber framework which was placed on a Teflon petri dish. The wet 3D PAN/LLTO nanofiber framework was first dried in air for 12 h and the above process was repeated for another side. Afterwards, CPEs were dried at 60 °C in a vacuum oven overnight to remove the residual solvent. At last, CPEs were named as PPE, PPLE1, PPLE2, and PPLE3 according to the mass ratio of PAN to LLTO, respectively. The electrolyte prepared directly from the slurry was named SPE by directly

forming a film on the surface of a stainless steel instead of PAN/LLTO nanofiber framework and using the same drying procedure.

2.4 Materials characterization

The morphology and energy dispersive spectrometry (EDS) maps of materials were obtained by field-emission scanning electron microscopy (FESEM, S-4800, Hitachi Ltd., Japan). X-ray diffraction (XRD) tests were conducted on a Rigaku-Ultima IV diffractometer to characterize the crystal structure of the CPEs, along with the 2θ range from 10° to 80°. Fourier transform infrared (FTIR) spectroscopy was performed under attenuated total reflectance (ATR)-FTIR mode using the Thermo Scientific Nicolet 6700 spectrometer. Thermogravimetric analysis (TGA) was performed via a TGA-Q5000IR instrument from 30 to 600 °C using a heating rate of 10 °C·min^{-1} in an N$_2$ atmosphere. Differential scanning calorimetry (DSC) measurements were carried out on a DSC Q1000 instrument from 20 to 120 °C in a nitrogen environment at 10 °C·min^{-1} ramp-up rates.

2.5 Electrochemical measurements

The ionic conductivity of CPEs from 30 to 80 °C was tested by assembling a SS/CPE/SS symmetric cell, the impedance frequency was changed from 100 mHz to 4 MHz via the Zahner Zennium electrochemical workstation. Consequently, the specific ionic conductivity (σ) values were calculated by Eq. (1):

$$\sigma = \frac{D}{R \times S} \tag{1}$$

where D is the thickness of the CPEs, R is the resistance value of CPEs obtained by the EIS test, and S is the area of the SS. The electronic conductivity (σ') of PPLE2 is also tested under the same conditions. In addition, the calculation was based on Eq. (2):

$$\sigma' = \frac{I_s \times D'}{U \times S'} \tag{2}$$

where I_s is the steady-state current, D' is the thickness of the PPLE2 CPE, U is the polarization voltage(1 V), and S' is the area of the SS.

Linear sweep voltammetry (LSV) was conducted from 2 to 6 V at a scan rate of 1 mV·s^{-1} by Ivium-n-Stat. The lithium-ion transfer number (t_{Li}^+) was calculated by Eq. (3):

$$t_{Li}^+ = \frac{I_s(\Delta V - I_0 R_0)}{I_0(\Delta V - I_s R_s)} \tag{3}$$

where ΔV is the polarization voltage (10 mV), R_0 and I_0 are the resistance and current before polarization, respectively,

R_s and I_s are the resistance and current after polarization, respectively.

To assemble a full battery for testing, the cathode material was fabricated by dissolving LiFePO$_4$ (LFP), PVDF, SP, and CPE into NMP at a mass ratio of 7:1:1:1, then the slurry was coated onto a carbon-coated aluminum foil and dried at 80 °C in a vacuum oven overnight. The mass loading of LiFePO$_4$ in the cathode was 1 mg·cm^{-2}. CR2025-type coin batteries were fabricated in an argon-filled glove box, and the charge/discharge tests of the batteries were performed between 2.5 and 4.2 V on a Neware battery testing system (BTS4000, China).

3 Results and discussion

The preparation process of PAN/LLTO-based CPE is shown in Fig. 1. Firstly, LLTO nanoparticles (Fig. 1a) were prepared by the solvothermal method. Then LLTO nanoparticles and PAN were dissolved in DMF together to prepare the precursor used for electrospinning (Fig. 1b). Thereby, the schematic structure of the prepared 3D PAN/LLTO nanofiber framework (Fig. 1c) was given with an SEM image. Finally, PAN/LLTO-based CPE (Fig. 1d) was prepared by the solution-casting method with the slurry.

SEM images of 3D PAN/LLTO nanofiber frameworks with different mass ratios of PAN to LLTO are given in Fig. 2a–d. The nanofibers in PNF exhibited a smooth surface with an average diameter of about 200 nm (Fig. 2e). Nonetheless, the uneven diameter distribution of nanofibers due to the incorporation of LLTO nanoparticles can be clearly observed in PLNF1 (Fig. 2b), which can be attributed to the fact that the addition of LLTO nanoparticles changes the surface tension of the Taylor cone formation during the electrospinning process. This problem can be effectively solved by further increasing the mass ratios of PAN to LLTO to 1:2. SEM image (Fig. 2c) and diameter distribution statistics (Fig. 2f) show that improved surface tension does not significantly increase or decrease the fiber diameter. Meanwhile, EDS mapping images of La, Ti, and O in PLNF2 were measured (Fig. 2g–i), these elements are evenly distributed on nanofibers, which indicates the uniform distribution of LLTO nanoparticles. In addition, the mapping images of PLNF1 and PLNF3 are also given in Fig. S1. However, when the mass of LLTO nanoparticles is further increased, large quantities of LLTO nanoparticles will not be uniformly dispersed and will agglomerate (Fig. 2d), which will lead to a decrease in the content of the organic–inorganic composite conductive interface, and cause the reduction of the ionic conductivity as well as poor electrochemical performance.

XRD patterns and FTIR spectra of materials are shown in Fig. 3. The crystalline phase of as-prepared LLTO nanoparticles was tested by XRD (Fig. 3a). All the diffraction peaks of the LLTO nanoparticles can be assigned to the cubic phase perovskite structure (JCPDS No. 87-0935). The inset showed the microstructure of the LLTO nanoparticles synthesized by the solvothermal method, with an average size of 70 nm.

To further reveal the changes of polymer crystallinity in CPEs, XRD tests were performed on pure PEO and prepared CPEs (Fig. 3b). The pure PEO shows two distinct
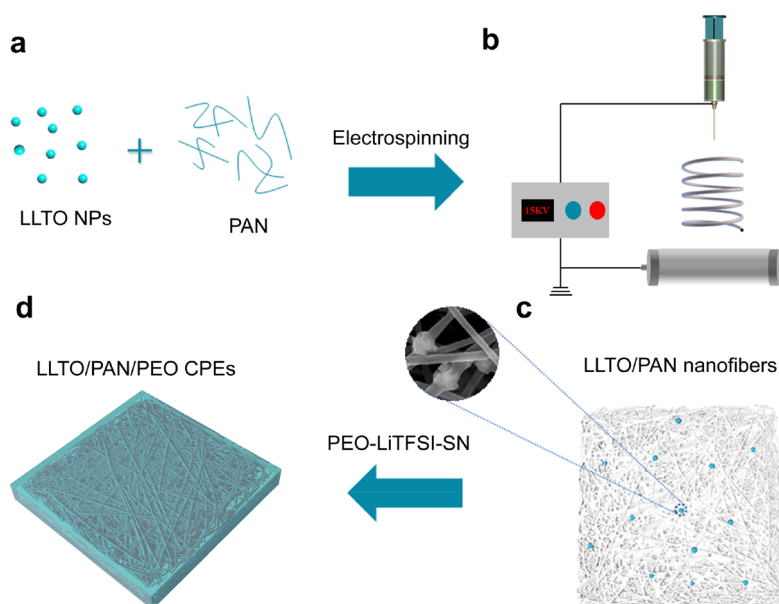

Fig. 1 **a** LLTO nanoparticles prepared by solvothermal method; **b** combination of PAN and LLTO nanoparticles for electrospinning; **c** 3D PAN/LLTO nanofiber framework; **d** PAN/LLTO-based CPE obtained by solution casting method
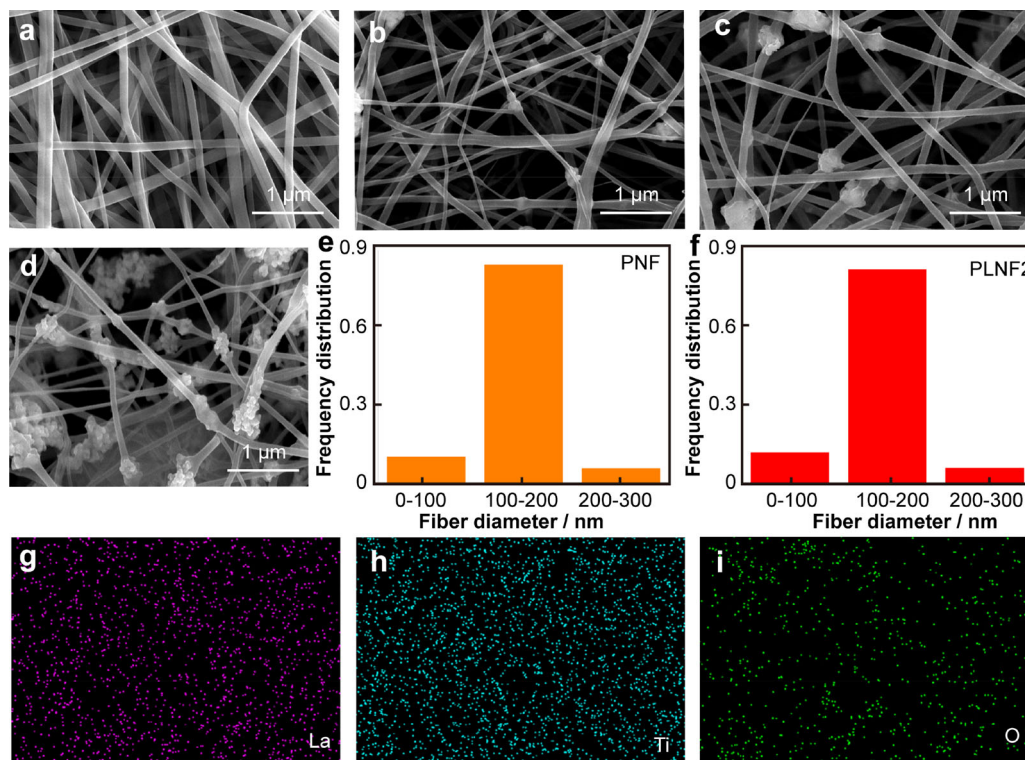
Fig. 2 SEM images of 3D PAN/LLTO nanofiber framework with different mass ratios of PAN to LLTO: **a** PNF, **b** PLNF1, **c** PLNF2, and **d** PLNF3; diameter distribution statistics of nanocomposite fibers: **e** PNF, and **f** PLNF2; **g–i** EDS mappings of La, Ti and O elements of **c**
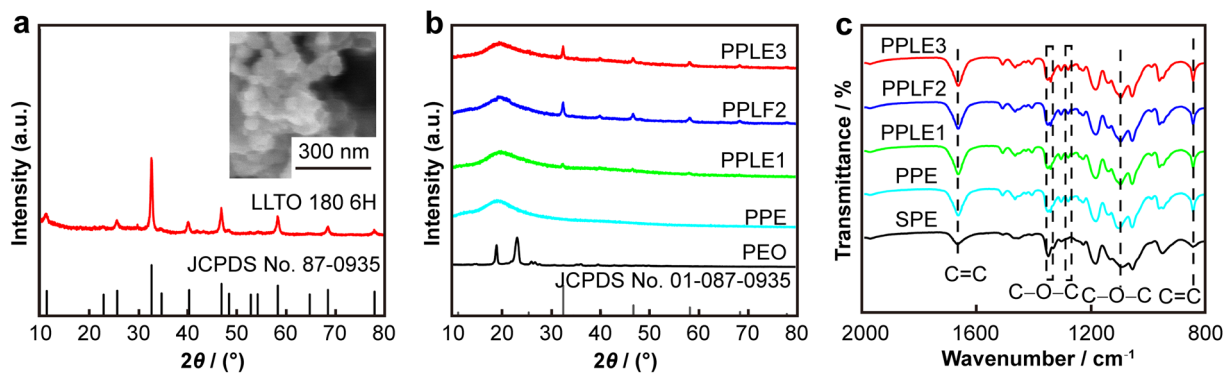

Fig. 3 **a** XRD pattern of LLTO nanoparticles with an inset SEM image; **b** XRD patterns of PEO and CPEs; **c** FTIR spectra of SPE and CPEs

characteristic diffraction peaks of PEO at 19.2° and 23.3°, and high crystallinity is considered not beneficial to the transmission of lithium-ions. Surprisingly, the peak of PEO at 23.3° disappeared in all CPE we prepared; meanwhile, the peak at 19.2° turns to an amorphous peak. The synergistic effect of SN and LLTO nanoparticles greatly reduces the crystallinity of PEO, which is necessary for the fast transmission of lithium ions. This result can be verified by DSC curves of PPE, PPLE2, and pure PEO in Fig. S2. As presented, the melting temperature (T_m) of pure PEO was

found at 70 °C; meanwhile, the endothermic peaks of PPE and PPLE2 shifted to a lower temperature (40 °C), which implies the synergistic effect of SN and LLTO in reducing the crystallinity of PEO.

FTIR spectra of SPE and CPE are presented in Fig. 3c, the peaks at 1670 and 840 cm^{-1} were ascribed to the stretch vibration of C = C. In addition, the new peak at 1340 cm^{-1} and enhanced peaks at 1280 and 1100 cm^{-1} were ascribed to the vibration of the –C–O group. These peaks can enhance the transmission of lithium ions [43].

As an important parameter of ASSLMBs, the thermal stability of CPEs is shown in Fig. S3. When Celgard starts to deform at 80 °C and fully shrink at 160 °C, PPLE2 can still maintain its original shape. Besides, compared with PLE, the addition of LLTO increases the decomposition temperature of PEO in PPLE2 to 350 °C from 320 °C (Fig. S4), which proves that the interaction between LLTO and polymers significantly improves the thermal stability of CPEs. Excellent thermal stability of CPEs can fundamentally solve the short circuit problems caused by the melting of the diaphragm in LIBs.

The temperature-dependent ionic conductivity plots and corresponding impedances of SPE and CPEs are displayed in Figs. 4a and S5. First of all, the ionic conductivity of all CPEs is higher than that of the SPE, indicating that the addition of a 3D PAN/LLTO nanofiber framework can construct a more complex hybrid conductive interface and 3D lithium-ion transmission channel, which is beneficial for lithium-ion transmission. Secondly, with the increase of LLTO content, the ionic conductivities of the CPEs first increase and then decrease due to the agglomeration of LLTO nanoparticles (Fig. 2d). The ionic conductivity reached a maximum among them when the LLTO mass fraction was twice to that of PAN for 9.87×10^{-5} S·cm^{-1} at 30 °C, and it meets the basic requirements of ASSLMBs applications. Meanwhile, the electronic conductivity (Fig. S6) of PPLE2 only reached 1.94×10^{-10} S·cm^{-1}, which is widely regarded as not conducive to the formation of lithium dendrites.

To characterize the electrochemical stability of the electrolyte, LSV curves (Fig. 4b) were measured through assembling Li/CPE/SS cells. As the picture shows, the current curve of the SPE rises quickly around 4.6 V (vs. Li$^+$/Li), which means that the PEO begins to decompose at the voltage and is determined as electrochemical window. By loading the SPE into the 3D PAN/LLTO nanofiber framework, the electrochemical stability of CPE has been improved to a certain extent. Especially, the current curve of PPLE2 did not fluctuate significantly between 2.0 and 4.8 V, illustrating that the addition of 3D PAN/LLTO nanofiber framework can efficiently improve the electrochemical stability of the electrolyte. The t_{Li}^+ of PPLE2 was measured by a direct current (DC) polarization method and the result (Fig. 4c) shows that PPLE2 had a high t_{Li}^+ of 0.41, which is much higher than that of PEO (0.11) [44]. We believed that unlike conventional nanofiller CPEs [45–50], lithium-ions can not only follow the molecular chain segments of PEO for rapid transfer, but also can make rapid jumps along the nanofibers after reaching the PAN/LLTO nanofibers in PEO/PAN/LLTO CPES, which is far greater than the transfer rate in PEO electrolytes alone. This special 3D lithium-ion transport channel synergistically enables fast lithium-ion transport, thus ensuring high ionic conductivity and excellent electrochemical performance of CPEs.

The growth of lithium dendrites in ASSLMBs has always been criticized. In order to verify the ability to inhibit the growth of lithium dendrites as well as the interface stability between CPE and lithium metal, galvanostatic cycling tests (Fig. 5a) were performed on Li/Li symmetric cells at 30 °C with a current density of 0.1 mA·cm^{-2}. It is obvious that the Li/Li symmetric cell with PLE exhibited a large polarization voltage and increased with time, and then a short circuit suddenly occurred at 200 h. However, Li/Li symmetric cell using PPLE2 could cycle stably for 1000 h without a short circuit and large voltage polarization. Besides, we found that the gradual increase of LLTO mass not only enhances the interfacial stability between electrolyte and lithium metal, but also significantly inhibits the growth of lithium dendrites. A gradually increasing polarization voltage and a short circuit at 320 h were also observed when using PL11 for assembling the Li/Li symmetric cell, indicating lithium dendrites pierce CPE. Compared with PL11, Li/PPLE3/Li sandwich cell demonstrates stable polarization voltage until 500 h and then begins to fluctuate instead of a short circuit. And it can be clearly seen that with the gradual increase of LLTO mass, the high mechanical strength of
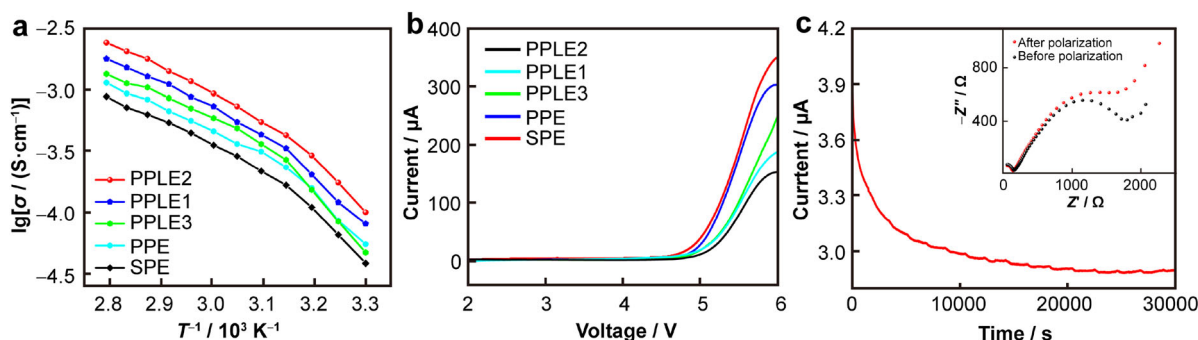

Fig. 4 a Arrhenius plots of SPE and CPEs; b LSV curves of SPE and CPEs; c Chronoamperometry curve of symmetric Li/PPLE2/Li cells and (inset) AC impedance spectra before and after polarization

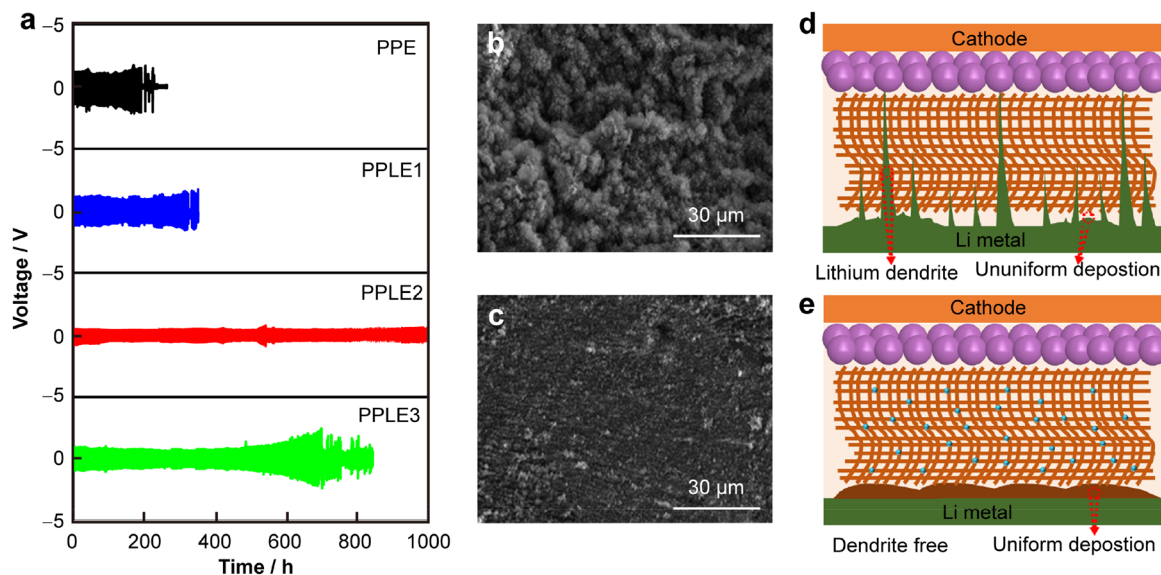**Fig. 5** **a** Long-cycling performance of Li/Li symmetric cells with CPEs; SEM images of Li metal surface **b** in Li/PLE/Li cell after a cycling short circuit and **c** in Li/PPLE2/Li cell after 1000 h cycling at 0.1 mA·cm^{-2}; illustration of **d** PLE and **e** PPLE2 to inhibit lithium dendrites

LLTO nanoparticles can significantly inhibit lithium dendrites and 3D PAN/LLTO nanofiber framework can effectively improve interface stability. By constructing CPEs with PAN/LLTO nanofiber framework and PEO, a 3D fast lithium-ion transport channel is achieved, which enables rapid transport of lithium-ion at the interface as well as in the interior of CPEs. Benefiting from this, an uniform distribution of lithium-ions on the surface of lithium metal is achieved, resulting in uniform deposition of lithium-ions. In addition, the high mechanical strength LLTO can also exert mechanical resistance and inhibit the growth of lithium dendrites.

Furthermore, Li/Li symmetric cells after cycles were disassembled in an argon-protected glove box, and the surface of the lithium metal after cycles was characterized by SEM. A great number of lithium dendrites and uneven lithium deposition (Fig. 5b) were observed on the surface with the lithium metal of Li/PLE/Li cell after a short circuit. However, only dense and uniform lithium depositions were observed on the lithium metal surface of Li/Li symmetric cells using PPLE2 after cycling for 1000 h (Fig. 5c), without obvious lithium dendrites, which is consistent with the previous galvanostatic cycling test results. We believed that the addition of LLTO nanoparticles can effectively increase the mechanical strength of the CPE itself, thus inhibiting the formation of lithium dendrites. A schematic diagram (Fig. 5d, e) is presented to illustrate the effect of how PLE and PPLE2 inhibit the growth of lithium dendrites.

Based on the above work, the LFP/CPE/Li full battery was further assembled to verify the feasibility of the prepared CPEs when used in ASSLMBs. Here, the rate performance test (Fig. 6a) was conducted with the C-rate calculated according to 1.0C = 170 mAh·g^{-1}. According to the charge and discharge curves (Fig. 6b), LFP/PPLE2/Li cells showed a specific discharge capacity of 152.9, 151.1, 139.7, and 115.9 mAh·g^{-1} at 0.1C, 0.2C, 0.5C, and 1.0C, respectively, which are significantly higher than other samples.

Long-cycling performances of LFP/CPE/Li batteries at 30 °C with 0.2C (Fig. 6c) and 0.5C (Fig. 6d) were also shown to characterize the cycle stability of the batteries. LFP/PPLE2/Li battery exhibited a high initial discharge capacity for 156.2 mAh·g^{-1} and maintained 146.9 mAh·g^{-1} after 100 cycles with the capacity retention rate of 97.4% at 0.2C (Fig. S7), similarly, the battery maintained 127.2 mAh·g^{-1} after 200 cycles with the capacity retention rate of 93.9% at 0.5C (Fig. S8). In comparison to PPLE2, the PLE electrolyte showed poor cycle stability performance with the capacity retention rate of 90.91% and 58.85% at 0.2C and 0.5C, respectively, indicating that PPLE2 had excellent long-cycling stability. Therefore, it can be concluded that the addition of 3D PAN/LLTO nanofiber framework is helpful to improve rate performance and long-cycling stability of the batteries, which were of great significance for the development of high-performance ASSLMBs. As shown in Table S1, we can also clearly see that the specific capacity of the LFP/
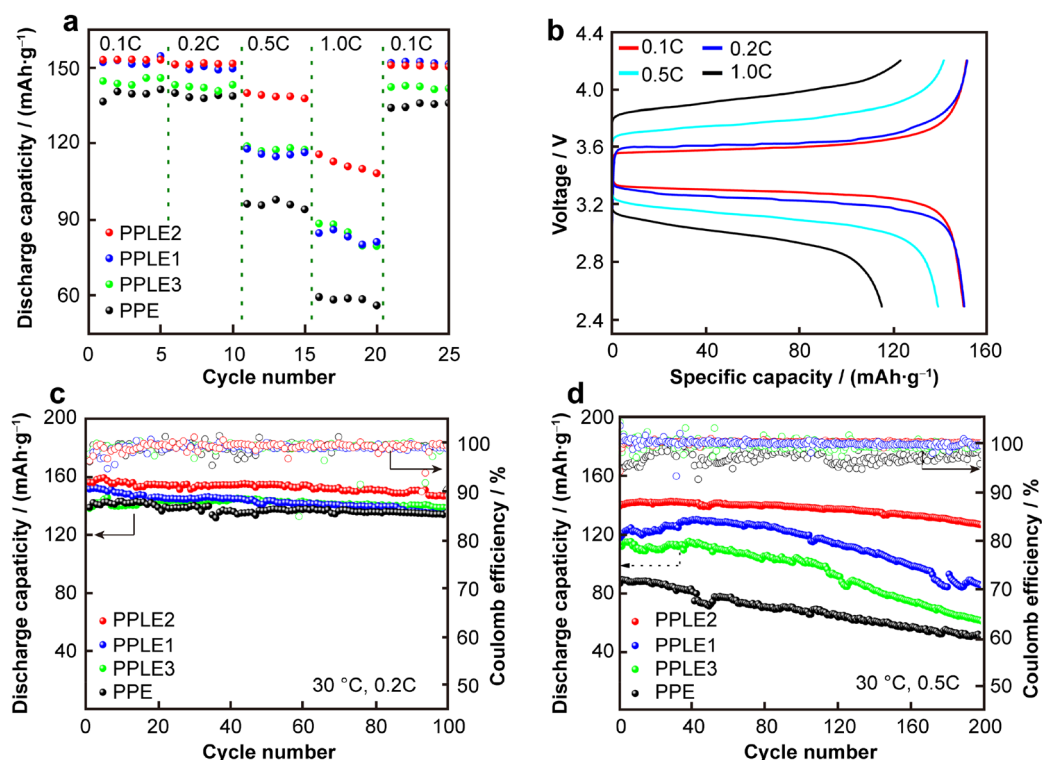
Fig. 6 **a** Rate capability of LFP/CPE/Li cells at 30 °C; **b** charge and discharge curves of LFP/ PPLE2/Li cell at 30 °C; long-cycling performance of LFP/CPE/Li batteries at 30 °C with different rates: **c** 0.2C, and **d** 0.5C
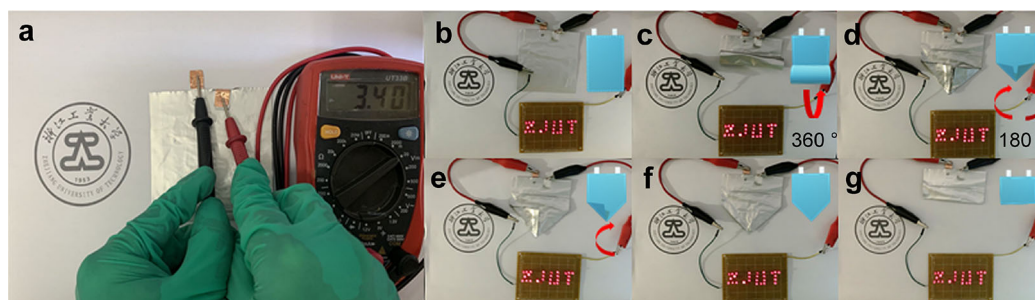

Fig. 7 **a** Open circuit voltage (OCV) test of a typical LFP/PPLE2/Li pouch cell; optical photos of the LFP/PPLE2/Li pouch cell for the safety performance test at **b** flat, **c** bending, **d** folded, **e** cut off one eighth, **f** cut off a quarter, and **g** cut off a half

PPLE2/Li battery is even higher than that of some other reported CPEs working at 60 °C.

The safety performance of the battery under harsh conditions was also an important factor that cannot be ignored in practical applications. Thus, a typical LFP/PPLE2/Li pouch cell was assembled in an argon-filled glove box. As shown in Fig. 7a, the open circuit potential (OCV) of the assembled LFP/PPLE2/Li pouch cell was 3.40 V. Subsequently, the pouch cell was tested under various harsh conditions (Fig. 7b–g). It can be seen that the pouch cell could operate well (ZJUT LED lamps matrix) under bending and folding. Even after direct cutting several times, the pouch cell could still work well without any fire

and short circuit, fully demonstrating the high safety performance of the LFP/PPLE2/Li pouch cell.

4 Conclusion

In summary, we designed a 3D PAN/LLTO nanofiber framework reinforced PEO electrolytes by electrospinning and solution casting method. By adjusting the ratio of LLTO to PAN, the CPE exhibits an ionic conductivity for about 9.87×10^{-5} S·cm^{-1} at 30 °C with a wide electrochemical window up to 4.8 V. The Li/Li symmetric battery using PPLE2 electrolyte could cycle stably for 1000 h

under 30 °C at 0.1 mA·cm^{-2} without a short circuit. Besides, the LFP/PPLE2/Li battery also exhibits excellent cycle stability with the capacity retention rate reach to 97.4% after 100 cycles at 0.2C and 93.9% after 200 cycles at 0.5C, respectively. Through the addition of the polymer/ceramic nanofiber framework and SN, the excellent electrochemical performance of ASSLMBs at room temperature is achieved. This work provides a new insight for the design of safe, high-performance room-temperature ASSLMBs.

Declarations

Conflict of interests The authors declare that they have no conflict of interest.

References

[1] Banerjee A, Wang X, Fang C, Wu EA, Meng YS. Interfaces and interphases in all-solid-state batteries with inorganic solid electrolytes. Chem Rev. 2020;120(14):6878.

[2] Hu J, He P, Zhang B, Wang B, Fan LZ. Porous film host-derived 3D composite polymer electrolyte for high-voltage solid state lithium batteries. Energy Storage Mater. 2020;26:283.

[3] Lu J, Liu Y, Yao P, Ding Z, Tang Q, Wu J, Ye Z, Huang K, Liu X. Hybridizing poly(vinylidene fluoride-co-hexafluoropropylene) with $Li_{6.5}La_3Zr_{1.5}Ta_{0.5}O_{12}$ as a lithium-ion electrolyte for solid state lithium metal batteries. Chem Eng J. 2019;367:230

[4] Meyer WH. Polymer electrolytes for lithium-ion batteries. Adv Mater. 1998;10(6):439.

[5] Jia M, Bi Z, Shi C, Zhao N, Guo X. Polydopamine coated lithium lanthanum titanate in bilayer membrane electrolytes for solid lithium batteries. ACS Appl Mater Interf. 2020;12(41):46231.

[6] Luo S, Zhao E, Gu Y, Huang J, Zhang Z, Yang L,Hirano SI. Rational design of fireproof fiber-network reinforced 3D composite solid electrolyte for dendrite-free solid-state batteries. Chem Eng J. 2021; 421(2):127771

[7] Huo H, Li X, Chen Y, Liang J, Deng S, Gao X, Doyle-Davis K, Li R, Guo X, Shen Y, Nan CW, Sun X. Bifunctional composite separator with a solid-state-battery strategy for dendrite-free lithium metal batteries. Energy Storage Mater. 2020;29:361.

[8] Siyal SH, Javed MS, Jatoi AH, Lan JL, Yu Y, Saleem M, Yang X. In situ curing technology for dual ceramic composed by organic-inorganic functional polymer gel electrolyte for dendritic-free and robust lithium-metal batteries. Adv Mater Interf. 2020;7(20):2000830.

[9] Yu H, Zhao J, Ben L, Zhan Y, Wu Y, Huang X. Dendrite-free lithium deposition with self-aligned columnar structure in a carbonate-ether mixed electrolyte. ACS Energy Lett. 2017;2(6):1296.

[10] Zou Z, Li Y, Lu Z, Wang D, Cui Y, Guo B, Li Y, Liang X, Feng J, Li H, Nan CW, Armand M, Chen L, Xu K, Shi S. Mobile ions in composite solids. Chem Rev. 2020;120(9):4169.

[11] Li S, Zhang SQ, Shen L, Liu Q, Ma JB, Lv W, He YB, Yang QH. Progress and perspective of ceramic/polymer composite solid electrolytes for lithium batteries. Adv Sci. 2020;7(5):1903088.

[12] Fan P, Liu H, Marosz V, Samuels NT, Suib SL, Sun L, Liao L. High performance composite polymer electrolytes for lithium-ion batteries. Adv Funct Mater. 2021;31(23):2101380.

[13] Yuan B, Wen K, Chen D, Liu Y, Dong Y, Feng C, Han Y, Han J, Zhang Y, Xia C, Sun A, He W. Composite separators for robust high rate lithium ion batteries. Adv Funct Mater. 2021. https://doi.org/10.1002/adfm.202101420.

[14] Kato Y, Hori S, Saito T, Suzuki K, Hirayama M, Mitsui A, Yonemura M, Iba H, Kanno R. High-power all-solid-state batteries using sulfide superionic conductors. Nat Energy. 2016;1(4):16030.

[15] Wang Y, Richards WD, Ong SP, Miara LJ, Kim JC, Mo Y, Ceder G. Design principles for solid-state lithium superionic conductors. Nat Mater. 2015;14(10):1026.

[16] Zheng C, Zhang J, Xia Y, Huang H, Gan Y, Liang C, He X, Tao X, Zhang W. Unprecedented self-healing effect of Li_6PS_5Cl-based all-solid-state lithium battery. Small. 2021. https://doi.org/10.1002/smll.202101326.

[17] Lee YG, Fujiki S, Jung C, Suzuki N, Yashiro N, Omoda R, Ko D-S, Shiratsuchi T, Sugimoto T, Ryu S, Ku JH, Watanabe T, Park Y, Aihara Y, Im D, Han IT. High-energy long-cycling all-solid-state lithium metal batteries enabled by silver–carbon composite anodes. Nat Energy. 2020;5(4):299.

[18] Ye L, Li X. A dynamic stability design strategy for lithium metal solid state batteries. Nature. 2021;593(7858):218.

[19] Murugan R, Thangadurai V, Weppner W. Fast lithium ion conduction in garnet-type $Li_7La_3Zr_2O_{12}$. Angew Chem Int Ed. 2007;46(41):7778.

[20] Thangadurai V, Narayanan S, Pinzaru D. Garnet-type solid-state fast Li ion conductors for Li batteries: critical review. Chem Soc Rev. 2014;43(13):4714.

[21] Su J, Huang X, Song Z, Xiu T, Badding ME, Jin J, Wen Z. Overcoming the abnormal grain growth in Ga-doped $Li_7La_3Zr_2O_{12}$ to enhance the electrochemical stability against Li metal. Ceram Int. 2019;45(12):14991.

[22] Liu Q, Geng Z, Han C, Fu Y, Li S, He YB, Kang F, Li B. Challenges and perspectives of garnet solid electrolytes for all solid-state lithium batteries. J Power Sour. 2018;389:120

[23] Xiang X, Liu Y, Chen F, Yang W, Yang J, Ma X, Chen D, Su K, Shen Q, Zhang L. Crystal structure and lithium ionic transport behavior of Li site doped $Li_7La_3Zr_2O_{12}$. J Eur Ceram Soc. 2020;40(8):3065.

[24] Li QH, Xu C, Huang B, Yin X. Sr^{2+}-doped rhombohedral $LiHf_2(PO_4)_3$ solid electrolyte for all-solid-state Li-metal battery. Rare Met. 2020;39(9):1092.

[25] Mong AL, Shi QX, Jeon H, Ye YS, Xie XL, Kim D. Tough and flexible, super ion-conductive electrolyte membranes for lithium-based secondary battery applications. Adv Funct Mater. 2021;31(12):2008586.

[26] Tang S, Guo W, Fu Y. Advances in composite polymer electrolytes for lithium batteries and beyond. Adv Energy Mater. 2021;11(2):2000802.

[27] Manthiram A, Yu X, Wang S. Lithium battery chemistries enabled by solid-state electrolytes. Nat Rev Mater. 2017;2(4):16103.

[28] Wan J, Xie J, Mackanic DG, Burke W, Bao Z, Cui Y. Status, promises, and challenges of nanocomposite solid-state electrolytes for safe and high performance lithium batteries. Materials Today Nano. 2018;4:1.

[29] Wei WQ, Liu BQ, Gan YQ, Ma HJ, Cui DW. Protecting lithium metal anode in all-solid-state batteries with a composite electrolyte. Rare Met. 2021;40(2):409.

[30] Fu X, Shang C, Yang M, Akinoglu EM, Wang X, Zhou G. An ion-conductive separator for high safety Li metal batteries. J Power Sources. 2020;475:228687

[31] Huo H, Li X, Sun Y, Lin X, Doyle-Davis K, Liang J, Gao X, Li R, Huang H, Guo X,Sun X. Li_2CO_3 effects: new insights into polymer/garnet electrolytes for dendrite-free solid lithium batteries. Nano Energy. 2020;73:104836

[32] Liu W, Lee SW, Lin D, Shi F, Wang S, Sendek AD, Cui Y. Enhancing ionic conductivity in composite polymer electrolytes with well-aligned ceramic nanowires. Nat Energy. 2017;2(5):17035.

[33] Zhu P, Yan C, Zhu J, Zang J, Li Y, Jia H, Dong X, Du Z, Zhang C, Wu N, Dirican M, Zhang X. Flexible electrolyte-cathode bilayer framework with stabilized interface for room-temperature all-solid-state lithium-sulfur batteries. Energy Storage Mater. 2019;17:220.

[34] Xu H, Zhang X, Jiang J, Li M, Shen Y. Ultrathin $Li_7La_3Zr_2O_{12}$@PAN composite polymer electrolyte with high conductivity for all-solid-state lithium-ion battery. Solid State Ionics. 2020;347:115227

[35] Zhu P, Yan C, Dirican M, Zhu J, Zang J, Selvan RK, Chung CC, Jia H, Li Y, Kiyak Y, Wu N,Zhang X. $Li_{0.33}La_{0.557}TiO_3$ ceramic nanofiber-enhanced polyethylene oxide-based composite polymer electrolytes for all-solid-state lithium batteries. J Mater Chem A. 2018;6(10):427

[36] Huo H, Chen Y, Luo J, Yang X, Guo X, Sun X. Rational design of hierarchical "ceramic-in-polymer" and "polymer-in-ceramic" electrolytes for dendrite-free solid-state batteries. Adv Energy Mater. 2019;9(17):1804004.

[37] Wan Z, Lei D, Yang W, Liu C, Shi K, Hao X, Shen L, Lv W, Li B, Yang QH, Kang F, He YB. Low resistance-integrated all-solid-state battery achieved by $Li_7La_3Zr_2O_{12}$ nanowire upgrading polyethylene oxide (PEO) composite electrolyte and PEO cathode binder. Adv Funct Mater. 2019;29(1):1805301.

[38] Li D, Chen L, Wang T, Fan LZ. 3D fiber-network-reinforced bicontinuous composite solid electrolyte for dendrite-free lithium metal batteries. ACS Appl Mater Interf. 2018;10(8):7069.

[39] Bi J, Mu D, Wu B, Fu J, Yang H, Mu G, Zhang L,Wu F. A hybrid solid electrolyte $Li_{0.33}La_{0.557}TiO_3$/poly(acylonitrile)

[40] membrane infiltrated with a succinonitrile-based electrolyte for solid state lithium-ion batteries. J Mater Chem A. 2020;8(2):706

[40] Hu S, Du L, Zhang G, Zou W, Zhu Z, Xu L, Mai L. Open-structured nanotubes with three-dimensional ion-accessible pathways for enhanced Li^+ conductivity in composite solid electrolytes. ACS Appl Mater Interf. 2021;13(11):13183.

[41] Famprikis T, Canepa P, Dawson JA, Islam MS, Masquelier C. Fundamentals of inorganic solid-state electrolytes for batteries. Nat Mater. 2019;18(12):1278.

[42] Huang F, Liu W, Li P, Ning J, Wei Q. Electrochemical properties of LLTO/fluoropolymer-shell cellulose-core fibrous membrane for separator of high performance lithium-ion battery. Materials. 2016;9(2):75.

[43] Zhang N, Wang G, Feng M, Fan LZ. In situ generation of a soft–tough asymmetric composite electrolyte for dendrite-free lithium metal batteries. J Mater Chem A. 2021;9(7):4018.

[44] Gao L, Li J, Ju J, Cheng B, Kang W, Deng N. Polyvinylidene fluoride nanofibers with embedded $Li_{6.4}La_3Zr_{1.4}Ta_{0.6}O_{12}$ fillers modified polymer electrolytes for high-capacity and long-life all-solid-state lithium metal batteries. Compos Sci Technol. 2020;200:108408

[45] Zhou W, Wang S, Li Y, Xin S, Manthiram A, Goodenough JB. Plating a dendrite-free lithium anode with a polymer/ceramic/polymer sandwich electrolyte. J Am Chem Soc. 2016;138(30):9385.

[46] Li Y, Xu B, Xu H, Duan H, Lü X, Xin S, Zhou W, Xue L, Fu G, Manthiram A, Goodenough JB. Hybrid polymer/garnet electrolyte with a small interfacial resistance for lithium-ion batteries. Angew Chem Int Ed. 2017;56(3):753.

[47] Bae J, Li Y, Zhao F, Zhou X, Ding Y, Yu G. Designing 3D nanostructured garnet frameworks for enhancing ionic conductivity and flexibility in composite polymer electrolytes for lithium batteries. Energy Storage Mater. 2018;15:46.

[48] Chen L, Li Y, Li SP, Fan LZ, Nan CW, Goodenough JB. PEO/garnet composite electrolytes for solid-state lithium batteries: from "ceramic-in-polymer" to "polymer-in-ceramic." Nano Energy. 2018;46:176.

[49] Zhou W, Wang Z, Pu Y, Li Y, Xin S, Li X, Chen J, Goodenough JB. Double-layer polymer electrolyte for high-voltage all-solid-state rechargeable batteries. Adv Mater. 2019;31(4):1805574.

[50] Gao L, Li J, Ju J, Wang L, Yan J, Cheng B, Kang W, Deng N, Li Y. Designing of root-soil-like polyethylene oxide-based composite electrolyte for dendrite-free and long-cycling all-solid-state lithium metal batteries. Chem Eng J. 2020;389:124478.